minerals

MDPI

Article

Exploring the Composition of Egyptian Faience

Francesca Falcone [1,2,3,4,*], Maria Aquilino [4] and Francesco Stoppa [1,2,3,4]

[1] Department of Psychological, Health and Territorial Sciences (DiSPuTer), G. d'Annunzio University Via dei Vestini, 66100 Chieti, Italy; fstoppa@unich.it
[2] Center for Advanced Studies and Technology (CAST), G. d'Annunzio University, 66100 Chieti, Italy
[3] Centro di Ateneo di Archeometria e Microanalisi (C.A.A.M.), G. d'Annunzio University, 66100 Chieti, Italy
[4] U.d'A analyTicAl High-Tech Laboratory (D.A.T.A.), G. d'Annunzio University, 66100 Chieti, Italy; maria.aquilino1990@gmail.com
* Correspondence: francesca.falcone@unich.it

Abstract: Egyptian Faience, a revolutionary innovation in ancient ceramics, was used for crafting various objects, including amulets, vessels, ornaments, and funerary figurines, like shabtis. Despite extensive research, many aspects of ancient shabti production technology, chemistry and mineralogy remain relatively understudied from the 21st to the 22nd Dynasty, belonging to a recovered 19th-century private collection. The fragments' origin is tentatively identified in the middle Nile valley in the Luxor area. Our study focused on a modest yet compositionally interesting small collection of shabti fragments to provide information on the glaze's components and shabti's core. We found that the core is a quartz and K-feldspars silt blended with an organic component made of plastic resins and vegetable fibres soaked with natron. The studied shabti figurines, after being modelled, dried, and covered with coloured glaze, were subjected to a firing process. Sodium metasilicate and sulphate compounds formed upon contact of the glaze with the silica matrix, forming a shell that holds together the fragile inner matrix. The pigments dissolved in the sodic glaze glass, produced by quartz, K-feldspars, and natron frit, are mainly manganese (Mn) and copper (Cu) compounds. The ratio $Cu_2O/CaO > 5$ produces a blue colour; if <5, the glaze is green. In some cases, Mg and As may have been added to produce a darker brown and an intense blue, respectively. Reaction minerals provided information on the high-temperature firing process that rapidly vitrified the glaze. These data index minerals for the firing temperature of a sodic glaze, reaching up to a maximum of 1050 °C.

Keywords: Egyptian Faience; shabti; Cu pigment; silica-body matrix; mineral neofaces; Scanning Electron Microscopy with Energy Dispersive Spectrometry (SEM-EDS); X-ray Powder Diffraction (XRPD)

check for updates

Citation: Falcone, F.; Aquilino, M.; Stoppa, F. Exploring the Composition of Egyptian Faience. *Minerals* **2024**, *14*, 586. https://doi.org/10.3390/min14060586

Academic Editors: Lluís Casas and Alberto De Bonis

Received: 2 April 2024
Revised: 29 May 2024
Accepted: 30 May 2024
Published: 31 May 2024

Copyright: © 2024 by the authors. Licensee MDPI, Basel, Switzerland. This article is an open access article distributed under the terms and conditions of the Creative Commons Attribution (CC BY) license (https://creativecommons.org/licenses/by/4.0/).

1. Introduction

This paper details the findings of a multi-analytical investigation into Egyptian Faience fragments of uncertain origin. According to Vandiver, Nicholson et al. and Kiefer [1–3], Faience materials were used to create various objects. The fragments display a range of features, including glaze and core composition, colour, inscriptions, and identification as Egyptian shabti figurines. The ambiguity regarding these materials' exact provenance and dating poses challenges in confirming their background. Nevertheless, because of the apparent connection between these fragments and their historical counterparts, their study could offer insights into the production techniques of Egyptian shabtis, thereby aiding in their dating and provenance determination. These objects, shaped like mummies, frequently depict agricultural tools such as hoes, baskets, and sacks in their painted or embossed hands, symbolising the shabti's role as a servant in the afterlife. Our goal is to explore the mineralogy and chemistry of these fragments better to understand the composition and history of these shabti figurines.

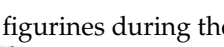
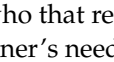
Egyptian Faience is the earliest high-tech ceramic fired in advanced kilns, and it consists of silica cores covered with a translucent blue-green glaze. The literature presents two

viewpoints regarding Egyptian Faience compositional material and production technology. Kaczmarczyk et al. and Shortland describe the Faience core as very friable and white [4,5]. Nicholson and Vandiver observed that the core matrix, skilfully modelled from silica silt with over 90% quartz, incorporated various compounds of calcium, sodium, potassium, magnesium, titanium, and aluminium [1,6]. They suggested Egyptian Faiences were crafted using autocementation, which involved self-glazing through chemical reactions during firing. First, the raw materials, primarily crushed quartz mixed with alkaline compounds and lime, were combined into a paste. The moulded figurines were left to dry, allowing them to harden slightly before firing, a process supported by Delfa et al.'s research on reproducing the glaze layer on Faience, confirming that ceramic samples were dried before the firing step [7]. Several chemical reactions occurred during firing, typically at temperatures between 800 and 1000 °C. The figurines were then allowed to cool slowly to prevent cracking and to solidify the glaze. Nicholson and Henderson's study provides insight into the production techniques of Egyptian Faience, suggesting that the microstructure of the core consists of discrete grains of quartz linked by a tiny film of glass, with the silica core containing crushed alkaline glaze (frits) and an organic moulding binder [2]. The core, whether stonepaste or fritware, features a robust composition that allows artisans to craft designs because of its durable nature and versatile moulding capabilities [6]. During firing, the organic binder volatilises, enabling a limited amount of clay and glass frit to form a melted glassy network that partially fills areas around the quartz crystals, creating a glass-supported porous structure [8–11]. Delfa et al., reproduced Faience glaze to support the thesis that ceramic samples were dried before the firing step [7].

Nicholson and Schneider suggest that the glaze was created from a mixture of tiny particles of silica, lime, copper minerals, and alkali mixed in water, which, during firing, gave the object its hardness and shiny, colourful appearance [6,11]. The alkali reacted with the silica to form a glassy phase on the surface, and through capillary action, it migrated to the surface carrying copper compounds, forming the glaze by efflorescence. Kakoulli and Siddall explained the glaze production techniques differently, affirming the use of Egyptian blue produced through the preliminary heating of copper raw minerals [8,9]. Egyptian blue is a pioneering synthetic pigment in ancient Egyptian art and decoration. This pigment contains cuprorivaite ($CaCuSi_4O_{10}$) obtained from quartz, copper ores like malachite, and a calcium carbonate crushed mixture followed by melting at a high temperature between 800 and 1000 °C. The melt was subsequently cooled as a glass and ground into a fine powder, producing an artificial pigment, as claimed by Frame et al. [10].

Using a multi-methodological archaeometric approach, we aim to enhance the understanding of Egyptian Faience. This approach illustrates the mechanisms regulating the chemical reactions between the glaze and matrix and reveals the use of plant fibres within the core [4,5].

2. Historical Framework

Shabti figurines are mummiform artefacts bearing the owner's name, titles, and funerary offerings for the deceased's *Ka*. These figurines may include texts about afterlife work, have a well-defined head, and carry various objects. The terminology evolves from shabtis to shawabtis and ushabtis. According to the studies of Schneider [11], the oldest word to identify these figurines is *SAbty.w* (shabti. w), written in the plural form and with the wood determinative  . Wood determinative could be related to the word shabti if we consider that they have the same root, the difference being that the latter has a mummiform figure as determinative  . The term *SAwAbty* (shawabty)  identified wood figurines during the 17th Dynasty. In the Third Intermediate Period, the term *wSbty*  (the who that responds) emerged, emphasising the role of the figurines in responding to their owner's needs in the afterlife [12]. *SAb* (food) also links shabti to sustenance, depicting it as the one who provides sustenance. In the First Prophet Pinedjem II's figurines, the term "*ushabti*" first appears in hieroglyphs of Chapter 6 in the

Book of the Dead, replacing "*shabti*" in the Late Period. Statuettes of Masaharta, Pinedjem I's son, feature a distinctive headband known as a "*seshed*", a characteristic of figurines from the 21st and 22nd dynasties. This feature provides dating. Shabtis have simplified forms and material uniformity in his period with ordinary terracotta and Faience. Shabti inscriptions become shorter and are written in a single column with the name and title of the deceased. The figurines turn into amulets with magical properties after this age. Table 1 is the summary of the principal features and evolution of shabtis.

Table 1. Materials used in the evolution of figurine production reflected by availability and symbolism.

Period	Dynasty	Materials	Inscriptions	Characteristics and Functions
Middle Kingdom ca. *1980–1760 BC*	11–12th Dyn.	Stone, less frequently, wood.	Rare inscriptions, some bear the name and title of the owner. Occasionally, the *shabti spell*.	Mummiform appearance: transition to *shabti*s as labourers in the afterlife, guided by the *shabti spell* [11,13].
Second Intermediate Period	17th Dyn.	Wood.	It may contain an offer formula.	The variant shawabty, made from Persea wood, is called a stick and has a simple and raw shape [14].
New Kingdom ca. *1539–1077 BC*	18th Dyn.	Hard rock-type granite and later alabaster were used.	Name and titles of the owner. *Shabti* spell.	The objects are crafted in the shape of mummies (mummiform) and often feature agricultural tools such as hoes, baskets, and sacks in their painted or embossed hands as part of their iconography, symbolising the shabti's role as a servant in the afterlife. [14,15].
	End of 18th–19th Dyn.	Wood and stone were replaced by ceramic and Faience.	Name and titles of the owner. *Shabti* spell.	The deceased wore the dress of daily life [16].
Third Intermediate Period ca. *1076–723 BC*	21–24th Dyn.	Faience was used frequently, rarely stone and wood.	The inscriptions are brief, with only Osiris's epithet and the deceased's title.	The *shabti supervisors* led groups of ten statuettes: 401 *shabti*s supervised by 36 reis. The term *ushabti* appeared for the first time. [12]
Late Period ca. *722–332 BC*	25th Dyn-2nd Persian Period.	Faience with inscriptions engraved. A dorsal pillar and trapezoidal base [9].	The *ushabti*s are inscribed with Chapter 6 of the *Book of the Dead*.	The strict rule of 401 figurines per tomb became flexible. The term *ushabti* was replaced *shabti* [15–19].

The chronology of all tables is referred to [1–19].

3. Materials and Methods

3.1. Materials

The university received 23 Egyptian Faience fragments from a fortuitous finding, part of a lost collection possibly from the 19th century AD (Figure 1). The owner guessed these may have come from Egypt and donated the samples to the university.

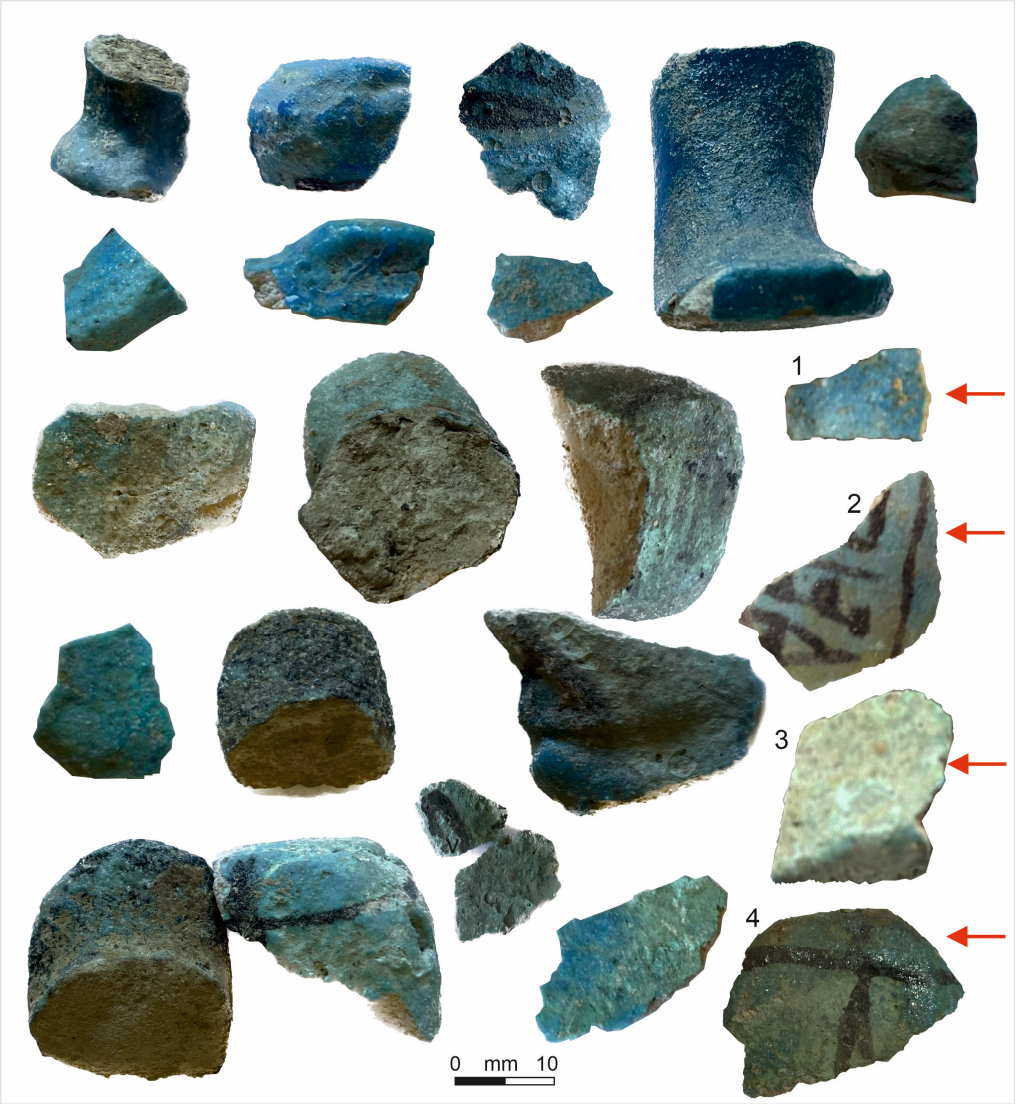


Figure 1. An image of a small collection of Egyptian Faience, as it arrived when generously donated to the university by an anonymous donor. The figure displays the fragments deemed representative and selected for archaeometric study, numbered 1–4.

The fragments of Faience were identified in shabti figurines based on morphological and typomorphic characteristics and recognisable inscriptions. The samples were identified as figurines of different sizes and parts of the back and front, distinguishable by inscriptions. The fragments were categorised into three groups, selecting the best representative sample based on the state of conservation, the differences in blue and green, and legible inscriptions.

3.2. Methods

An in-depth, combined analysis of the materials from the macro to the nanoscale was carried out to identify the compositions appropriately. The samples were prepared for investigation using an optical microscope (OM), Scanning Electron Microscopy with Energy Dispersive Spectrometry (SEM-EDS), and X-ray Powder Diffraction (XRPD).

Small parts of the selected samples were taken from fresh areas of the samples to avoid alteration of the investigated materials. Subsequently, as the material to be studied was very fragile, it was encapsulated in epoxy resin under vacuum conditions. The surface of the resin-encapsulated samples was smoothed and polished to allow for further analysis.

All the chemical and mineralogical data are semi-quantitative and thus provide a general indication of the composition and differences among the various parts that make

up these figurines. Their chemistry and mineralogy are complex because of the organic and glass components, which are impossible to reveal with a single technique. For these reasons, we used a multi-analytical approach.

Optical Microscope (OM)

Twenty-three samples were initially considered for preliminary analysis based on their typomorphic features. However, after a meticulous examination, four samples were identified as particularly representative and thus suitable for a comprehensive investigation. These four samples were selected based on detailed optical microscopy (OM) screening and categorised according to their matrix and glaze as follows: blue glaze (sample 1), green glaze (sample 2), and inscriptions and decorations (samples 3 and 4). Our selection process was guided by the imperative to preserve the integrity of the samples for future research. In the field of Cultural Heritage diagnostics, it is essential to minimise the use of material and apply such methods only when absolutely necessary, as mandated by the Ministry of Cultural Heritage of Italy (MIC). The four selected samples best met these stringent criteria, ensuring both their representativeness and preservation. Therefore, we focused our investigation on these four samples, employing both destructive and microdestructive analyses, including SEM-EDS (resin and sanding) and XRPD. This approach allowed for thorough analysis while adhering to the highest standards of conservation and scientific rigour.

The observations of the Egyptian shabti samples were carried out using Optech Stereomicroscopes (Zoom LFZ, U.d'A analyTicAl High-Tech Laboratory (D.A.T.A.), G. d'Annunzio University, 66100 Chieti, Italy) equipped with an Optech K71857 EX6-C3 camera. First, an investigation into the conservation state of the constituent materials of the object was conducted. The observation was carried out on the intact specimen on the outer surface of the glaze and the inner part, i.e., the body matrix. Subsequently, cross-sectional observations were also carried out perpendicular to the object previously encased in resin and polished. The cross-sectional analysis allowed for using the glaze and inner core to study the vesiculations, layering, minerals, and inclusions for the glaze. For the matrix, texture, minerals, and porosity were investigated.

The reflected optical microscope (OM) examination revealed poor preservation, especially in the pronounced lack of cohesion in the matrices of samples 1 and 3. The glaze surface shows porosity, gaps (seen in sample 1 in Figure 2), recrystallisation, salt efflorescence, and encrustation. Some glaze sections are partially detached, revealing micro-cracks and conchoid fractures. Sample 1 is predominantly blue-green, sample 2 features a blue-green colour with brown inscriptions, sample 3 has a lighter green glaze, and sample 4 shares a brown decorative motif with sample 1 (Figure 2).

Reconstructing the original positions of the small fragments using the 4 selected samples was undoubtedly a challenging task. The positions of samples 1 and 3 in the original shabti figurine remained difficult to determine. In contrast, features such as the hieroglyphics on sample 2 and a well-preserved decorative element on the rear of sample 4 allowed for precise placement. This progress offers a hopeful glimpse into the possibility of piecing together the intricate puzzle and advancing our understanding of the overall structure. Figure 3 shows a shabti (Figure 3A) on the front side [14].

The complete inscription (Figure 3B) was compared with the remains of the inscription from sample 2. The two hieroglyphs decrypted represented the name of *Wsir God* (Figure 3C). This writing variant was used during the New Kingdom and the Third Intermediate Period. Figure 3D shows the shabti on the back side, which was used to compare the seshed headband tied at the back (Figure 3E) of sample 4. This sashed is related to the 21st–22nd Dynasty feature [7–9].

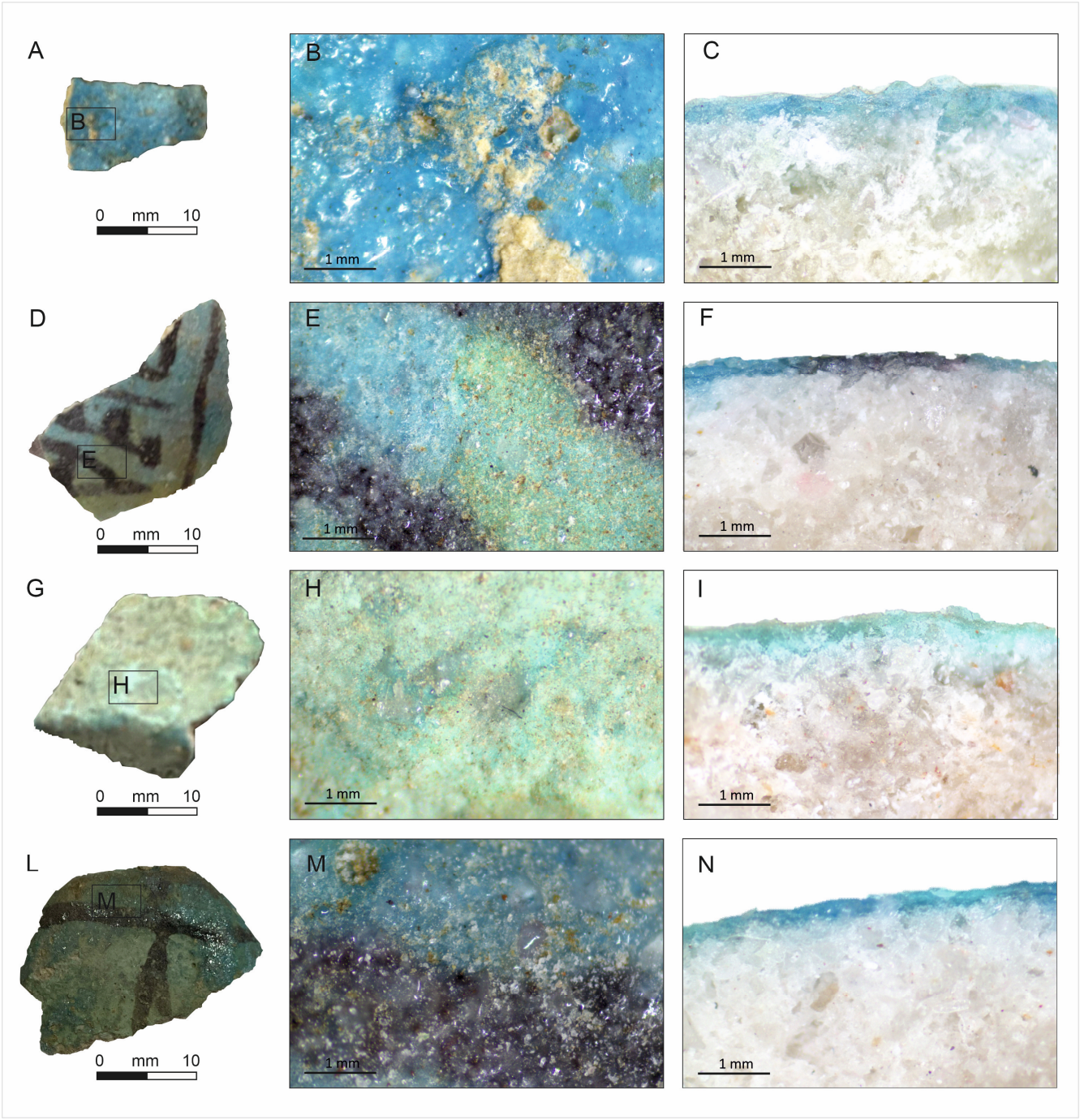


Figure 2. Samples were observed under an optical reflected light microscope (4.5X). Images (**A**), (**B**), and (**C**) are related to sample 1; (**D**), (**E**), and (**F**) are related to sample 2; (**G**), (**H**), and (**I**) are related to sample 3; and (**L**), (**M**), and (**N**) are related to sample 4. (**A**) Sample 1; (**B**) inset in A showing the coating (glaze) on an altered blue-greenish background and the presence of pores and gaps; and (**C**) glaze and core in the section of sample 1. (**D**) Whole sample 2; (**E**) inset in D showing glaze coating with brown inscriptions; and (**F**) section of sample 2. (**G**) Whole sample 3; (**H**) inset in G; and (**I**) cross section of samples 3. (**L**) Sample 4; (**M**) inset in L showing brown inscriptions; and (**N**) section of sample 4.

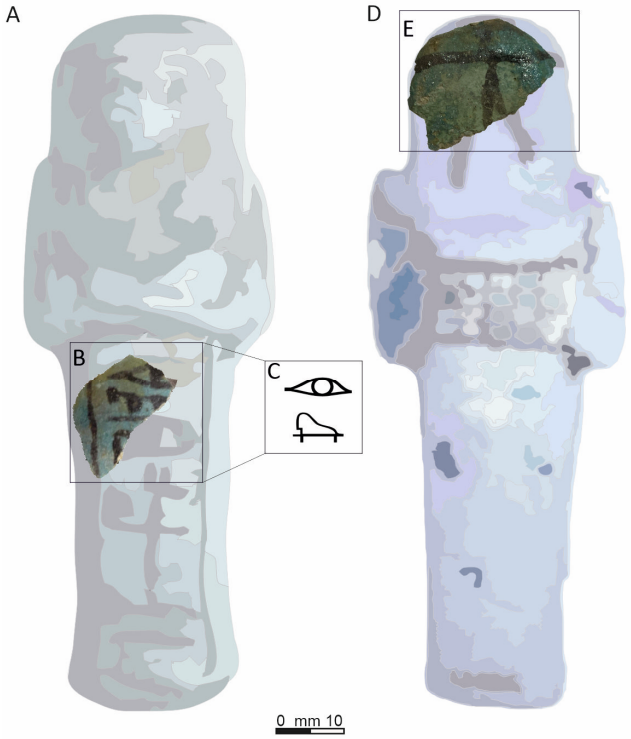


Figure 3. (**A**–**D**) Two examples of shabti [14] with decorations like those of the analysed fragments. (**B**) Sample 2, Shabti with a hieroglyphic inscription located in the exact position in the figurine; (**C**) inscription; (**D**) mummiform shabti in Faience with a seshed headband tied at the back; and (**E**) sample 4 with a seshed headband tied at the back.

3.3. Scanning Electron Microscopy with Energy Dispersive Spectrometry (SEM-EDS)

In addition to optical microscopy, we conducted comprehensive studies using advanced techniques. The Phenom XL scanning electron microscope (G2, software Pro Suite, U.d'A analyTicAl High-Tech Laboratory (D.A.T.A.), G. d'Annunzio University, 66100 Chieti, Italy) with microanalysis (SEM-EDS) was used to investigate the glaze layer's thickness, morphology and chemistry, core area, and interaction zone. Energy Dispersive spectrometry (EDS) analysis provided semi-quantitative insights. The analysis error is 2–3% for the principal oxides, and the detection limit is about wt% 0.1. The error percentage was calculated using a range of mineral standards of barite 2%, calcite 3%, and fluorite 1.3%. The detection limit was also checked based on mineral and artificial standards. Investigations were conducted to analyse the shabti object's layered structure and chemical composition. Two investigations were conducted at this stage, one on the intact sample and the other on the resin-embedded polished section.

(1) For the intact specimen's external glaze surface, the analysis was performed under conditions of low vacuum at 35–40 Pa, an accelerating voltage of 20 kV, a beam current of 65 mA, a working distance of 850 µm, and a live time of chemical analysis of 60 s. The aim was to determine the qualitative microstructural characteristics of the fragments coated with carbon.

(2) The section sample embedded in resin and polished was coated with carbon, and the analysis was performed in a high vacuum. We analysed points with a 2- to 4-micron spot and 15 kV working distance of 850 µm. In addition, we performed compositional maps measuring 0.8 × 0.8 mm during two and a half hours of analysis.

3.4. X-ray Powder Diffraction (XRPD)

Powder XRD analyses were carried out using the diffractometer Bruker (D2 Phaser, U.d'A analyTicAl High-Tech Laboratory (D.A.T.A.), G. d'Annunzio University, 66100 Chieti, Italy). This technique allows for the detailed examination of the crystallographic

structure of the sample. The acquisition parameters used in the XRPD data were Cu-K alpha (1.540598 Å) radiation generated at 30 kV and 15 mA in an exploratory interval between 3 and 70 2θ, a step of 0.1°, and a scan rate of 0.15°/s and with recording times set at one hour. Once the diffractogram was obtained, background subtraction and indexing of peak with semi-quantitative analysis were performed using EVA-Bruker software. XRD EVA software is a vital tool in X-ray diffraction (XRD) analysis, a technique used to scrutinise the crystal structure of materials by examining the diffraction patterns generated when X-rays interact with a crystalline sample. EVA software facilitates data analysis, visualisation, and interpretation by collaborating with XRD instruments. Its functionalities encompass preprocessing raw XRD data (e.g., background subtraction, smoothing, normalisation), identifying diffraction peaks indicative of specific crystalline phases, quantifying phase composition, refining crystal structure parameters, visualising diffraction patterns and crystal structures, and exporting processed data and analysis outcomes.

4. Descriptions and Results

4.1. Scanning Electron Microscopy with Energy Dispersive Spectrometry (SEM-EDS) and XRPD Matrix

SEM-EDS analysis of sample cross-sections allowed for detecting pristine, reaction, and alteration minerals. Specifically, the sample cores are similar as they contain abundant crushed quartz, minor K-feldspar, gypsum, calcite, hematite, magnetite, and sphene. They also include remnants of cotton, linen fibres, and straw fragments soaked in a natron solution [20]. The essential components and their relative abundance are displayed in Figure 4 and Table 2, respectively. The sample grain size is in the silt category (62.5 μm–2 μm).

Table 2. The mineral phases identified through X-ray Powder Diffraction Rietveld method analysis include contributions from glaze fragments, which are not entirely separable from the matrix.

Mineral	Chemical Formula	Mineral Phases Abundance %			
		#1	#2	#3	#4
Quartz	SiO_2	70.5	74.7	76.4	73.9
Cuprorivaite	$CaCuSi_4O_{10}$	4.50	2.20	5.50	3.10
Magnetite	Fe_3O_4	bdl	1.30	bdl	1.80
Atacamite	$ClCu_2H_3O_3$	2.60	bdl	1.10	1.30
Gypsum	$CaSO_4$	4.60	2.90	7.10	2.40
Calcite	$CaCO_3$	4.80	1.00	2.60	1.81
Hematite	Fe_2O_3	bdl	0.90	bdl	0.68
Sphene	$CaTiSiO_5$	3.20	2.50	3.90	2.80
Manganite	$MnO(OH)$	bdl	6.30	bdl	5.11
Orthoclase	$KAlSi_3O_8$	9.70	8.20	3.40	7.30

Numbers are expressed in wt% values of mineral phase composition; bdl: below the detection limit.

To identify valuable natural fibres, it is necessary to specify their typical characteristics, such as plant of origin, e.g., cotton comes from the cotton plant (Gossypium). Cotton fibres typically range from about 1 to 2.5 cm. Another point is the diameter of the fibres, where cotton fibres are generally thinner than linen [21–23]. The texture and appearance of cotton fibres are generally creamy white and have a soft, fluffy feel. Absorbency is an important characteristic. Both cotton and linen are absorbent fibres, but cotton has a higher absorbency rate than linen. Regarding strength and durability, linen fibres are generally more robust and durable than cotton fibres.

The most valuable and apparent features are highlighted between cotton and linen on the microscopic scale of the SEM-EDS. Cotton has a cylindrical and spiral ribbon shape and a larger diameter than linen fibres, which displays a "*bamboo*" shape (Figure 4). The characteristics of the fibres obtained in the SEM-EDS analyses are illustrated in Figure 3, which were revealed to be predominantly cotton. It was impossible to analyse the organic composition of organic matter using EDS, but when we analysed the fibres, we found that

they were soaked in potassium and sodium salts. Based on our knowledge of Egyptian technologies, we guess that this feature is typical of mummy bandages.

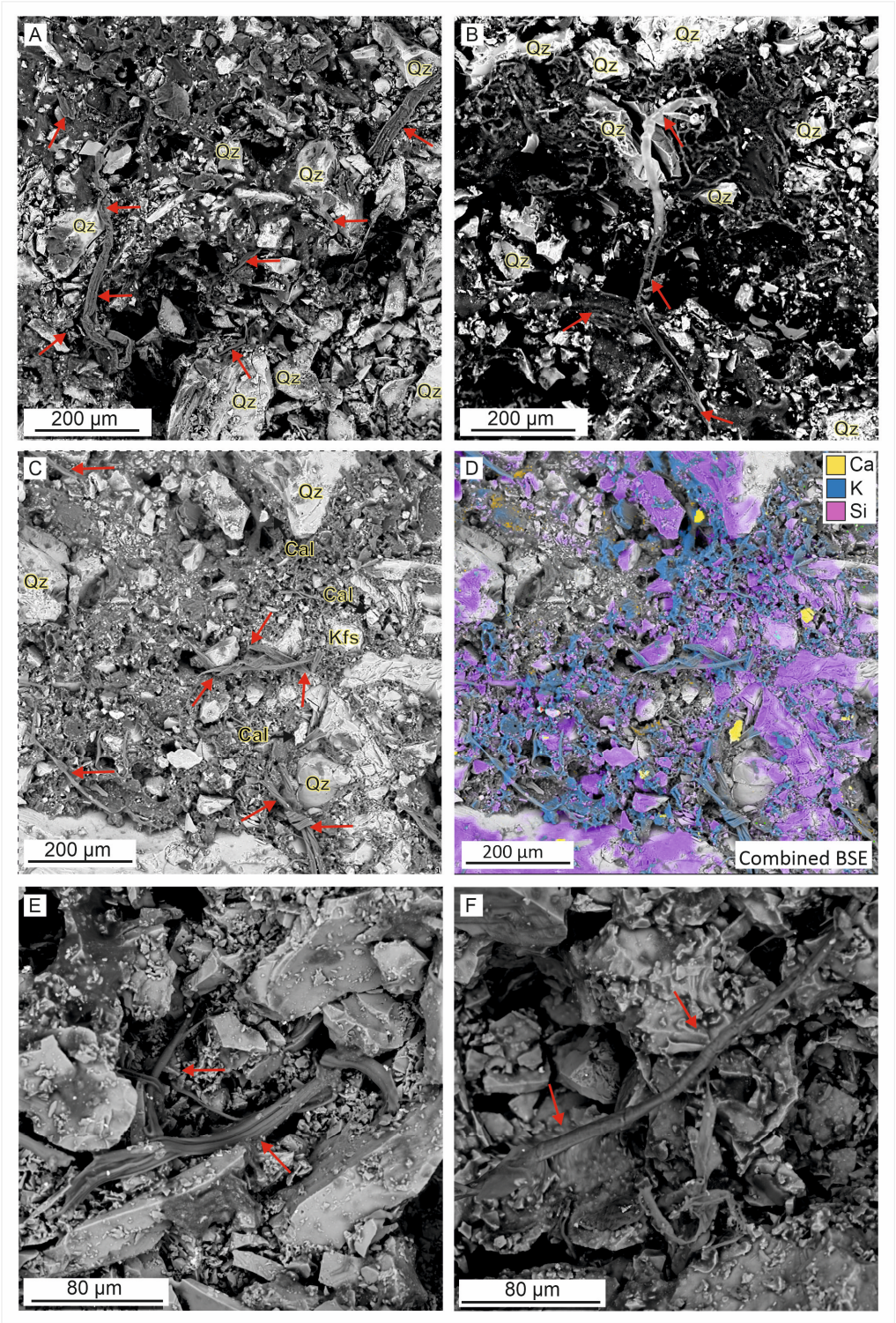


Figure 4. SEM-EDS analyses of core samples were investigated; the red arrow indicates vegetable fibres. (**A**) The core of sample 1; (**B**) the core of sample 2; (**C**) the greyscale imaging of sample 3; and (**D**) the combined BSE imaging of sample 3. Organic structures allow for the differentiation of cotton fibres from flax. (**E**) The typical spiral ribbon shape of cotton fibres and (**F**) the typical "*bamboo*" shape of flax fibres. Mineral abbreviations in the figure: Cal–calcite; Kfs–K-feldspar; Qz–quartz.

4.2. Minerals by XRPD and SEM-EDS

X-ray Powder Diffraction analyses provided crucial information on the core and glaze of the samples (Figure 5). Combining the SEM-EDS and the XRPD analyses allowed us to discriminate the minerals in the glaze and matrix. However, based on surface analysis, it was possible to understand glaze minerals, core minerals, and new phases.

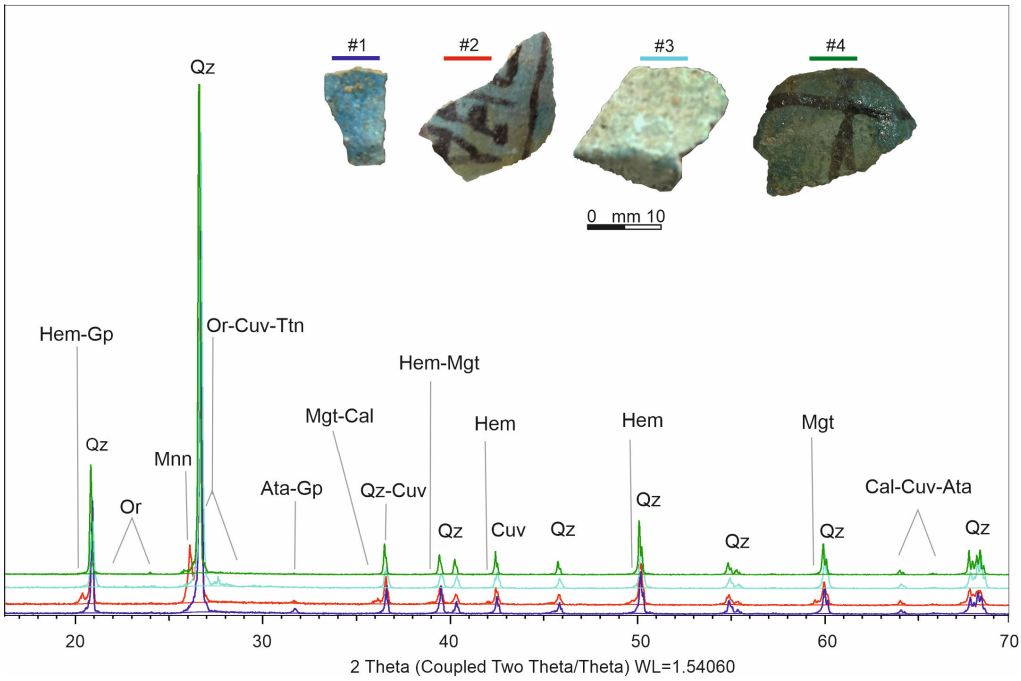


Figure 5. XRPD diffraction patterns of the samples (core and glaze). The deep blue diffraction pattern is for sample 1; the red diffraction pattern is for sample 2; the red diffraction pattern is for sample 3; and the green diffraction pattern is for sample 4. Mineral abbreviations are Ata–atacamite, Cal–calcite, Cuv–cuprorivaite, Gp–gypsum, Or–orthoclase, Hem–hematite; Mgt–magnetite; Mnn–manganite; Ttn–titanite; Qz–quartz. The Laurence N. Warr 2021 IMA abbreviation defines Minerals in the figure.

The identification of crystalline phases based on X-ray Powder Diffraction data, shown in Table 2, was confirmed by SEM-EDS chemical analysis of the core and glaze.

4.3. Glaze Glass

The glaze of the samples was analysed in two ways as follows: the external surface of the freshest areas and the inner part of the glaze, which was incorporated in resin and polished. SEM-EDS analysis of the altered glaze glass surface revealed relevant composition variations compared with the fresh glass (Table 3, alteration average of sample 1). The composition of the altered glass aligns with the formation of soluble salts such as halite, sodium chloride, gypsum, aluminium–iron hydroxides, and calcium sulphate encrustations.

The fresh glaze displays variations in composition across different colours and sample types (refer to Table 3, Figure 6, and Supplementary Table S1: Chemical results of analysed samples). The analyses reveal some alteration and dispersion in various compositional variations. Nonetheless, it remains feasible to differentiate among various groups, noting significant distinctions between surface and inner glaze compositions.

Table 3. Composition analyses of glasses in the glaze including core, surface, and different colour types.

Point Analysis	Sample	SiO_2	Al_2O_3	FeO	MnO	MgO	CaO	Na_2O	K_2O	As_2O_3	Cu_2O	Cl	SO_3
Surface glaze	#1Blue	83.3	0.24	bdl	bdl	2.59	2.26	2.10	0.09	7.48	1.97	2.59	bdl
	#2 Blue	85.4	0.26	bdl	bdl	1.79	6.51	1.51	0.14	1.89	1.91	1.79	0.20
	#2 Brown	82.3	0.31	bdl	3.10	2.58	6.07	1.58	bdl	2.20	1.07	2.58	bdl
	#3 Green	88.4	bdl	bdl	bdl	0.63	9.13	0.48	bdl	1.23	bdl	0.63	0.17
	#4 Blue	80.9	0.49	0.27	bdl	0.46	5.34	1.10	0.93	5.62	1.19	0.46	0.26
	#4 Brown	81.9	0.38	0.26	1.00	1.39	5.24	1.21	0.11	6.02	1.12	1.39	bdl
	* Alteration	53.7	7.89	5.40	bdl	1.16	5.64	14.1	3.43	bdl	1.59	3.59	2.70
Core glaze	#1Blue	83.7	0.22	bdl	bdl	0.04	2.34	2.42	1.95	bdl	7.39	1.94	bdl
	#2 Blue	85.2	0.78	bdl	bdl	0.18	1.67	7.20	0.99	bdl	2.75	1.13	bdl
	#2 Brown	80.4	1.13	bdl	2.95	0.64	1.33	7.45	1.71	bdl	2.95	1.18	bdl
	#3 Green	85.6	0.20	bdl	bdl	bdl	0.91	10.6	0.49	bdl	1.41	0.65	bdl
	#4 Blue	80.9	1.52	0.31	bdl	0.15	0.79	5.75	1.68	0.33	7.43	0.90	bdl
	#4 Brown	81.8	1.24	0.47	1.46	0.23	1.61	5.77	1.03	bdl	4.99	1.15	bdl
Average glaze	All types	83.6	0.59	0.09	0.66	0.16	1.65	6.03	1.36	0.08	4.30	1.25	0.03
	Blue	83.2	0.91	0.13	bdl	0.13	1.61	4.91	1.55	0.25	5.43	1.51	0.08
	Brown	81.6	0.88	0.21	2.13	0.38	1.72	6.13	1.38	0.03	4.04	1.13	bdl
	Green	87.0	0.10	bdl	bdl	bdl	0.77	9.84	0.49	bdl	1.32	0.33	0.08
Norm *. Values	Blue	1.06	1.22	1.38	0.09	0.83	1.08	0.82	1.36	3.67	1.42	1.37	1.50
	Brown	1.01	1.52	1.44	5.86	3.50	1.46	1.18	1.16	0.33	1.15	1.20	bdl
	Green	1.09	0.92	0.88	bdl	bdl	0.84	1.87	0.40	bdl	0.34	0.25	14.5

Values are expressed in wt%, * alteration average, and * normalised values (see Figure 6).

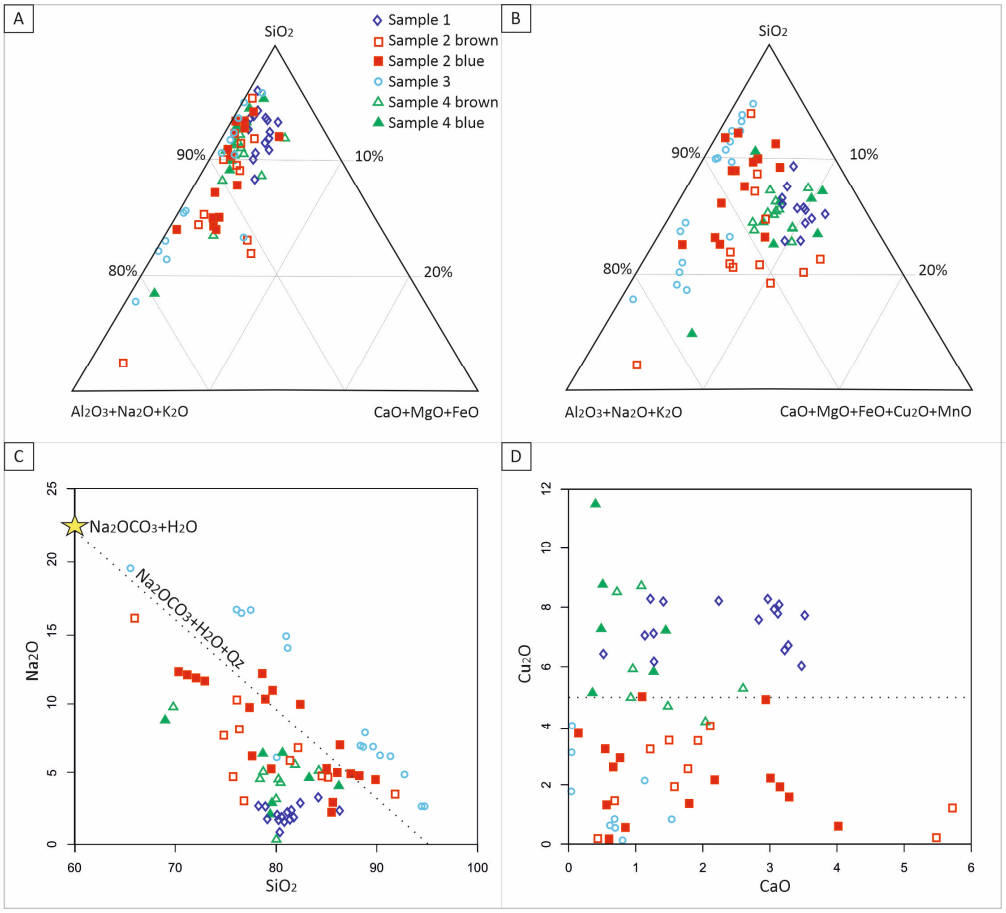


Figure 6. Diagrams of the inner glaze composition. (**A**) Ternary diagram of $SiO_2/Al_2O_3+Na_2O+K_2O/CaO+MgO+FeO$ (after Tite, 1997); (**B**) ternary diagram of $SiO_2/Al_2O_3+Na_2O+K_2O/CaO+MgO+FeO+Cu_2O+MnO$ (plus pigments); (**C**) binary diagram of Na_2O vs. SiO_2, where the regression line represents the degree of natron saturation of the glass in the glaze natron/quartz, with a maximum of 35% natron added; (**D**) CuO vs. Ca, where the dividing line represent two different compositions referring to high Cu glazes (samples 2–3) and low Cu glazes (samples 1–4). The legend and symbols are in the figure.

The glass base composition consists of silicon dioxide (SiO_2), making up approximately 84%, followed by sodium oxide (Na_2O) at around 6%, cuprous oxide (Cu_2O) at approximately 4.3%, calcium oxide (CaO) at 1.7%, potassium oxide (K_2O) at 1.4%, and chloride ions (Cl^{1-}) at 1.2%. All other components are present in quantities less than 1%. Consequently, the average glass can be classified as cuprous sodic.

Figure 6A,B show the glass composition in the glaze where some general differences among the four samples are visible (Figure 6). A general trend points to an Al_2O_3 + Na_2O + K_2O component, whereas the role of the pigment component is depicted in Figure 6B. A pretty sharp difference between the brown and blue glazes for the manganese contribution is apparent (Figure 6B). In Figure 6B, the green glaze glass and blue glaze glass of sample 2 are plotted on the left side, whereas all the others form a cluster in the centre of the diagram. The brown-coloured glaze glass is positioned on the centre-right side of the diagram.

Figure 6C shows the natron saturation degree based on Harcker diagram classification. Sample 3 trends above the line linking the SiO_2 (quartz) content with the Na_2O content of natron (more than 35%). Sample 2's blue glaze glass falls on the quartz–natron line. Sample 1 clusters are well below the line and have a lower Na_2O content (under-saturated in natron).

Figure 6D effectively distinguishes samples based on their Cu_2O/CaO ratio. Samples 1 and 4 exceed a ratio of 5, while samples 2 and 3 fall below it, clearly depicted in the graph. The higher copper content in samples 1 and 4 separates them from samples 2 and 3. Additionally, brown samples tend to lie below the graph's division line, attributed to decreased copper content as manganese content increases in their chemical composition.

The glasses in various differently coloured glazes do not differ much from the average, indicating that the mixture used as a base for creating the glaze had a relatively homogeneous composition. More tiny compositional differences produced by adding pigments in various compositions were investigated, normalising the analyses to the average of 93 analyses and revealing significant differences for some elements (Figure 7).

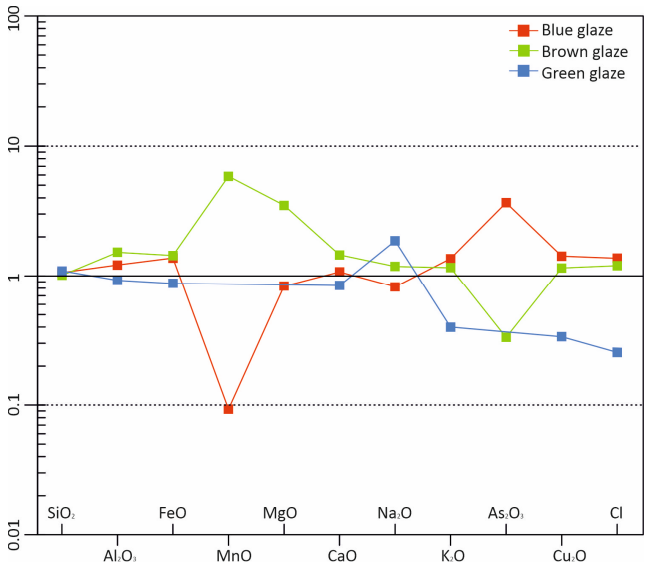


Figure 7. A spider diagram normalised based on the average glass glaze composition of the three glaze colouration types.

The Si content is uniform, and the Al, Fe, Ca, and Na content show minimal variation and are relatively similar to the average composition. Blue glaze glass exhibits a negative spike of MnO and positive spikes of As_2O_3. Green glaze glass features a positive spike of Na_2O and negative spikes of K_2O, CuO, As_2O_3, and Cl. Brown glaze glass stands out because of a notable increase in MnO and MgO and a negative spike of As_2O_3, setting it apart from all the other colours. The normalised values are the average values of the

analyses performed on the same types of glass (e.g., brown, green, blue glaze) divided by the average of all analyses.

The numerical data are shown in Table 3 and Supplementary Table S1; a graphical representation is shown in Figure 7.

5. Discussion

5.1. Matrix–Core

The shabtis' primary material, silt (62.5 µm–2 µm), contains quartz and K-feldspar, with intentional additions of calcite. Calcite was added, as we found it in discrete, sharp angular fragments dispersed in the matrix, not as incrustation filling the gaps between the vugs (Figure 4D). The calcite primary phase can be used to determine the maximum firing temperature. The composition of CO_2+CaO completes decoupling from 650° to 900°C. Magnetite, hematite, and sphene (heavy minerals) indicate a selective choice of river sediment deposit exposed to vigorous water currents able to remove the clay component, leaving heavy minerals, emphasising the meticulous nature of shabti production [24–26]. A sensible percentage of Na_2CO_3 and $NaH(CO_3)$ (natron), including sodium chloride, sodium carbonate, and sodium sulphate, was also added, as demonstrated by chemical analyses. The investigation reveals that natron salts permeate the linen and cotton fibres within the core cotton and linen based on the structures observed under the microscope (see Section 4.1, Figure 4E,F) [22–27].

Interestingly, our shabti body core resembles a cob rather than a stonepaste. According to Miller et al. and Stokes [26,28], the cob's adaptability makes it popular across cultures for various applications, including artistic designs. In the first stage, we assume the cob was desiccated before firing through exposure to sunlight and air. Adding non-dehydrated organic material during firing could compromise the object's integrity because of water expansion. The tiny fibres detected by SEM-EDS analysis appear to be a deliberate addition to the paste and come from the discarded mummy bandages. We guess the fibres from mummy bandages may indicate that the Faience workshop was sited near mummification sites. We think this is an interesting new fact in Egyptology, and we supported this fact by making a comparison with the cob, which is well known for the realisation of several artefacts in antiquity.

Furthermore, we do not think the fibres are due to contamination, as they are intricately mixed with the crystalline fragments of the core. Also, we found no trace of fibres on the surface of the samples. In the second stage, organic binders such as Arabic gum were evaporated after the coating and initial firing. In the third stage, the coating was partially melted, forming a glaze. During firing, a sturdy shell composed of glass and minerals resulting from the reaction between the core and glaze held the delicate core (Figure 8) [28]. Figure 8 shows the difference in the texture of the sample in the cross-section between the core and glaze.

The chemical data suggest that the reaction between the core (quartz) and the glaze (sodic melt) was fluxed by a mixture of sodium salts, primarily sodium carbonate decahydrate ($Na_2CO_3 \cdot 10H_2O$), sodium bicarbonate ($NaHCO_3$), and sodium sulphate (Na_2SO_4). Sodium silicate is formed by the reaction of silicon dioxide (SiO_2) and sodium hydroxide (NaOH). The chemical reaction is as follows (Equation (1)):

$$SiO_2 + 2NaOH \rightarrow Na_2SiO_3 + H_2O \quad (1)$$

The reaction produces a complex chain of metastable phases and H_2O, CO_2, and SO_2 as volatile byproducts. Many other phases found in the contact, such as gypsum ($CaSO_4$), can be obtained (Equation (2)):

$$2Ca(HCO_3)_2 + 2SO_2 \rightarrow 2CaSO_4 + 2H_2O + CO_2 \quad (2)$$

The reaction of silica (SiO_2) with sodium bicarbonate $NaH(CO_3)$ and sodium hydroxide (NaOH), along with sodium sulphate and SO_2 produces sodium nesosilicate Na_2SiO_3, sodium sulphate (Na_2SO_3), carbon dioxide CO_2, and water H_2O (Equation (3)):

$$SiO_2 + 2NaH(CO_3) + 2NaOH + (SO_2)^{2-} \rightarrow Na_2SiO_3 + Na_2SO_3 + 2(CO_2) + 2H_2O \quad (3)$$

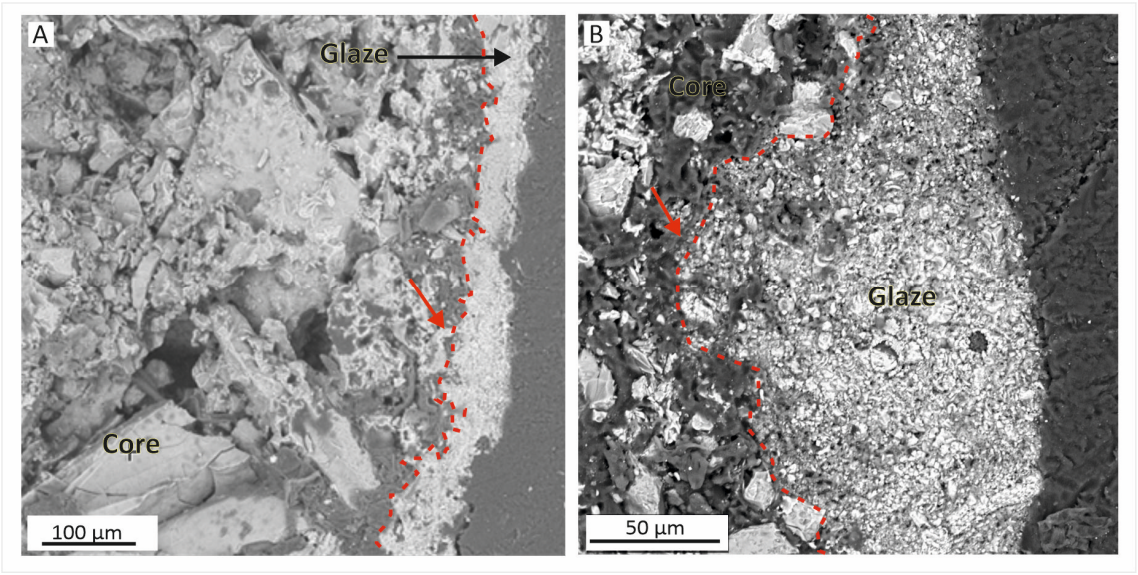


Figure 8. SEM images of a polished section: (**A**) sample 1 and (**B**) sample 4. The red dotted line highlighted by the red arrows, delineates the reaction shell between the core-matrix and the glaze.

5.2. Glaze

The row materials that form the frit to produce the glaze are mainly quartz, K-feldspars, and natron [2,3], supporting the analyses discussed in this paper. As defined by Moorey [25], the fritting process was vital in transforming soluble salts into insoluble ones, breaking down carbonates, sulphides, chlorides, and hydroxides and forming a complex mass of sintered silicates. K-feldspars and the silica plus natron flux reaction produce an atomic amorphous silicate medium (soda glass) plus volatile exsolution (Equation (4)):

$$KAlSi_3O_8 + SiO_2 + NaHCO_3 + Na_2CO_3 \rightarrow xK^{1+} + yNa^{1+} + zAl^{3+} + wSi^{4+} + 4CO^2 + 8H_2O \quad (4)$$

We guess that all the Na derives from natron, K derives from K-feldspars, and Si from quartz. The original compounds including cuprorivaite and manganite, serving as pigmenting agents, are common in this glaze [24,27–33]. Cuprorivaite ($CaCuSi_4O_{10}$), a calcium–copper silicate mineral, was the first synthetic pigment created by the Egyptians. A mixture of quartz sand and copper compounds like malachite or azurite is needed to produce Egyptian blue. Copper ores are found at *Um* and *Samiuki*, about 200 km southeast of *Luxor*. Cu compounds are added to calcium oxide and natron. Then, the mixture is heated and ground into a fine powder for pigment. We guess this is precisely the case in our analysis. Manganite (Mn hydroxide) deposits are famously known from *Sinai* in the *Bogma* district, but more minor occurrences are found in the *Halaib district* in Upper Egypt. All these raw materials were readily available in the ancient commercial trade of Egypt [34].

Surface glaze alterations resulted in salt compounds like atacamite, carbonates, halite, and sulphates, typical secondary phases due to alteration. Atacamite (copper chloride) was also detected in all the samples, but number 2. Atacamite ($Cu_2Cl(OH)_3$) is an alteration of Cu compounds such as cuprorivaite [32,34]. Regarding the formation of atacamite, let us also consider frits. The Egyptians were known to make natron frits with Cl-rich layers on the surface, as this halide can only be incorporated in small quantities into natron glass or glazes. The glaze must absorb sodium chloride salts (NaCl) to form atacamite. NaCl was used in various stages of the mummification process. It was often applied to the body or

used as part of the embalming materials to further aid in desiccation and preservation. In addition, attacamite could form by secondary alteration of copper phases with Cl^- ions in the presence of H_2O [35,36]. The reaction between cuprorivaite and sodium chloride to form atacamite can be represented as follows (Equation (5)):

$$CaCuSi_4O_{10} + 6NaCl \rightarrow 2Cu_2Cl(OH)_3 + Na_2SiO_3 + CaCl_2 \quad (5)$$

This reaction involves the exchange of ions between cuprorivaite ($CaCuSi_4O_{10)}$ and sodium chloride (NaCl), forming atacamite ($Cu_2Cl(OH)_3$), sodium silicate (Na_2SiO_3), and calcium chloride ($CaCl_2$). The atacamite/Cl ratio is higher in the inner glaze. Cl may derive from NaCl and possibly be associated with natron adsorbed by the fibres in the core that migrate towards the surface with time. The fibres are presumed to originate from discarded mummy bandages. The intricate relationship between mineralogy and natron-soaked fibre alteration is evidence of the fragment's ancient origin and authenticity [37] (Table S1: Chemical results of analysed samples, in Supplementary Materials).

6. Technology of Production

In Egyptian shabtis, the core was crafted using locally available minerals bound together by organic components, especially plant gums like gum Arabic and organic fibres. The combinations of these materials allowed for obtaining the desired consistency and workability. The manufacturing process involved compressing the plastic mixture into two moulds, which were then pressed together, shaped, and joined to form the final shabti [28,38,39]. After drying and glaze coating, the shabtis were fired at high temperatures. During the initial firing stage, the resin or organic binders were thermally decomposed at approximately 200–250 °C, evaporating through the pores of the core [25–30]. After evaporation of the organic binder, the mineral crystals remained interwoven with the vegetable fibres. With further temperature increase, the glaze melted and reacted with the outer layer of the core, forming a shell of neso-silicates of sodium. After cooling, this shell held the friable core of the object. Research indicates that shabtis underwent final firing within the temperature range of 870 °C to 920 °C [40,41]. There is no amount of flux or clay inside the cob, unlike when sintering the glass and forming interstitial glass. This phenomenon is observed in the firing reactions of typical stonepaste, but this was not found in our samples.

Cuprorivaite may form at low temperatures below 742 °C if flux-like plant ashes (K_2OH) are added [42]. However, with sodic flux, the temperature may be near 870–920 °C. Calcite completely dissociates at 800–1050 °C and dissolves in the glass, exsolving CO_2 [43]. Thus, we estimate that the glaze firing occurred at a temperature between 920 and 1050 °C. Although we know that wood ash was generally used [44,45], we ruled it out in this case since it would add calcium and potassium, while we found that the glaze is sodic, as visible in the diagrams (Figure 6).

Studies on the Ptolemaic shabti period reveal the use of cobalt and copper compounds as blue or blue-green pigments [38–48]. Usually, arsenic's presence coincides with cobalt's presence, which imparts a blue hue. Kaczmarczyk's contribution to the glaze study established the presence of cobalt in Egypt as a colouring agent and copper [47,48]. Our study confirmed the presence of copper in blue-green glaze, but no traces of cobalt were detected, which were probably below the detection limit of the instrumentation. Arsenic was detected instead (Table 3, Figure 7). This type of glaze colour differs from 10th-century Iranian ceramic productions in which cobalt was detected in association with copper [44,45]. The copper pigment glaze resulted in a vibrant blue-green colour, depending on the Cu_2O to CaO ratio, with the copper content yielding blue and a lower copper content producing green (Figure 6D). The alkali content played a crucial role, producing a high proportion of glass and diluting cuprorivaite crystals for lighter blue shades.

7. Conclusions

1. Our study centred on a modest yet compositionally interesting collection of shabti fragments and aimed to delve deeper into the glaze's material components and shabtis' inner core. Through chemistry and mineralogy examination, we discovered that the core comprises a silica-dominant silt mixture blended with organic substances, vegetable fibres, and natron additives. The identification of cotton fibres highlights the hitherto rarely detected Egyptian Faience associated with linen. This intricate blend facilitated the creation of ushabti figurines that underwent a series of processes, including modelling, drying, colouring with glaze, and firing.
2. Furthermore, examination of the shabti revealed a single firing event with minimal impact on the body, suggesting a relatively short firing time and insufficient flux salts in the matrix. Glaze composition analysis confirmed the presence of sodic silica glass with low potassium content, indicating a firing temperature between 920 °C and 1050 °C.
3. The pigments predominantly consisted of manganese (Mn) and copper (Cu) compounds, with the potential addition of Mg and As for specific colour variations. The Cu/Ca ratio is crucial to give a blue or green colour. Upon contact with the silica matrix, sodium metasilicate and sulphate compounds form a protective shell, ensuring cohesion within the fragile matrix.
4. Our study gives new chemical and mineralogical data and unravels some oddities in shabti production techniques, shedding light on the multifaceted nature of Egyptian crafting and its significance in ancient Egyptian civilisation.

Supplementary Materials: The following are available online at https://www.mdpi.com/article/10.3390/min14060586/s1, Table S1: Chemical results of analysed samples.

Author Contributions: Conceptualisation, F.F. and F.S.; methodology, F.F.; software, F.F.; validation, F.F. and F.S.; investigation and formal analysis, F.F.; resources, F.S.; instrumental resources, F.F. and F.S.; data curation, F.F. and F.S.; original draft preparation, F.F., M.A. and F.S.; writing—review, F.F. and F.S.; writing—editing, F.F.; figure curation, F.F.; supervision, F.S. All authors have read and agreed to the published version of the manuscript.

Funding: This research received no external funding.

Data Availability Statement: The data are contained within this article.

Acknowledgments: The analytical study in this paper was carried out in the D.A.T.A.-U.D.A. High-Technology Analysis Laboratory at the G. D'Annunzio University of Chieti, Italy.

Conflicts of Interest: The authors declare no conflicts of interest.

References

1. Vandiver, P.B.; Kingery, W.D. Egyptian Faience, The First High-Tech Ceramic. In *Ceramics and Civilisation III: High-Technology Ceramics. Past, Present and Future*; Kingery, W.D., Ed.; American Ceramics Society: Columbia, OH, USA, 1987; pp. 19–34.
2. Nicholson, P.T.; Henderson, J. *Ancient Egyptian Materials and Technology*; Cambridge University Press: Cambridge, UK, 2000; pp. 195–224, ISBN 0521452570.
3. Kiefer, C.; Allibert, A. Pharaonic Blue Ceramics: The Process of Self-Glazing. *Am. J. Archaeol.* **1974**, *24*, 107–117.
4. Kaczmarczyk, A.; Hedges, R.E.M. *Ancient Egyptian Faience: An Analytical Survey of Egyptian Faience from Predynastic to Roman Times*; Aris & Phillips: Warminster, UK, 1983.
5. Shortland, A.J.; Tite, M.S. Technological study of Ptolemaic—Early Roman Faience from Memphis, Egypt. *Archaeometry* **2005**, *47*, 31–46. [CrossRef]
6. Nicholson, P.T. *Egyptian Faience and Glass*; Shire Publications LTD.: Buckinghamshire, UK, 1993.
7. Delfa, S.L.; Formisano, V.; Ciliberto, E. Laboratory Production of Egyptian Faiences and Their Characterisation. *J. Cult. Herit.* **2008**, *9*, e113–e116. [CrossRef]
8. Kakoulli, I. Egyptian blue in Greek painting between 2500 and 50 BC. In *From Mine to Microscope: Advances in the Study of Ancient Technology*; Shortland, A., Freestone, I., Rehren, T., Eds.; Oxbow Books: Oxford, UK, 2009; pp. 101–112.
9. Siddall, R. Mineral Pigments in Archaeology: Their Analysis and the Range of Available Materials. *Minerals* **2018**, *8*, 201. [CrossRef]

10. Frame, L.; DeSordao, D.B.; Chiang, Y.C.; Vandiver, P. Methods of Faience Manufacture in Antiquity: Investigation of Colorants and Technological Processes. In *Materials Issues in Art and Archaeology VIII*; Vandidver, P.B., McCarthy, B., Tykot, R.H., Ruvalcaba-Sil, J.L., Casadio, F., Eds.; MRS Proceedings; Cambridge University: Cambridge, UK, 2011; Volume 1319, p. 43.
11. Schneider, H. *Shabtis: An Introduction to the History of Ancient Egyptian Funerary Statuettes with a Catalogue of the Collection of Shabtis in the National Museum of Antiquities at Leiden*; National Museum of Antiquities: Leiden, The Netherlands, 1977.
12. Rosmorduc, S. Sesh Documentation. Available online: http://jseshdoc.qenherkhopeshef.org (accessed on 12 June 2014).
13. Aubert, J.F.; Aubert, L. *Statuettes funéraires égyptiennes du département des Monnaies, Médailles et Antiques*; Éditions de la Bibliothèque Nationale de France; Bibliothèque Nationale de France-BNF: Paris, France, 2005. [CrossRef]
14. Janes, G. The Shabti collections 5. In *A Selection from the Manchester Museum England*; The Amadeus Press: Huddersfield, UK, 2012; 500p, ISBN 978-0-9566271-5-5.
15. Gama, A. Os Servidores Funerários da Coleção Egípcia do Museu Nacional: Catálogo e Interpretação. Ph.D. Thesis, Universidade Federal do Rio de Janeiro, Rio de Janeiro, Brazil, 2008.
16. Janes, G. Shabtis a Private View. In *Ancient Egyptian Funerary Statuettes in European Private Collections*; Éditions Cybèle: Paris, France, 2002.
17. Aubert, J.F. *Statuettes Égyptiennes: Chaouabtis, Ouchebtis*; Librairie d'Amérique et d'Orient Adrien Maisonneuve: Paris, France, 1974.
18. Stewart, H.M. *Egyptian Shabtis Buckinghamshire*; Shire Publications: London, UK, 1995.
19. Brancaglion, J. *Manual de Arte e Arqueologia do Egito Antigo II*; Sociedade dos Amigos do Museu Nacional: Rio de Janeiro, Brazil, 2004.
20. Hornung, E.; Krauss, R.; Warburton, D.A. *Ancient Egyptian Chronology*; Brill: Boston, MA, USA, 2006.
21. Ahmed, E.H. Brief of Natural Fibers in Historical Textiles Manufacturer. *Trends Text. Eng. Fash. Technol.* **2022**, *6*, 765–767. [CrossRef]
22. Carbonaro, A.B.; Caruso, R.; Greco, V.; El-Aguizy, O.; Ali, M.F.; Gambino, G.L.; Giuffrida, A.; Ciliberto, E. First evidence of fractionation on stable organic carbon isotopes in ancient Egyptian linen textile fibress during degradation. *J. Cult. Heritage* **2023**, *63*, 194–200. [CrossRef]
23. El Messiry, M.; Mohsen, S.A. Characterisation of Egyptian cotton fibres. *J. Fibres Text. Res.* **2013**, *38*, 109–113.
24. Lee, L.; Quirke, S. Painting Materials. In *Ancient Egyptian Materials and Technology*; Nicholson, P.T., Shaw, I., Eds.; Cambridge University Press: Cambridge, UK, 2000; pp. 104–120.
25. Moorey, P.R.S. *Materials and Manufacture in Ancient Mesopotamia: The Evidence of Archaeology and Art. Metals and Metalwork, Glazed Materials and Glass*; BAR International Series 237; Bar Publications: Oxford, UK, 1985.
26. Miller, A.; Johnson, B.; Garcia, C. Enhancing Cob Material Properties with Fibres and Lye Treatments. *J. Sustain. Constr.* **2000**, *15*, 124–137.
27. Henderson, J. *Ancient Glass: An Interdisciplinary Exploration*; Cambridge University Press: Cambridge, UK, 2013; ISBN 9781139021883. [CrossRef]
28. Stocks, A. Derivation of Ancient Egyptian Faience Core and Glaze Materials. *Antiquity* **1997**, *71*, 179–182. [CrossRef]
29. Tite, M.S.; Freestone, J.C.; Rimson, M. Egyptian Faience: An investigation of production methods. *Archaeometry* **1983**, *25*, 17–27. [CrossRef]
30. Aramaki, S.; Roy, R. Revised phase diagram for the system Al_2O_3—SiO_2. *J. Am. Ceram. Soc.* **1962**, *45*, 229–242. [CrossRef]
31. Kilikoglou, V.; Vekinis, G.; Maniatis, Y.; Day, P.M. Mechanical performance of quartz-tempered ceramics: Part I. Strength and toughness. *Archaeometry* **1998**, *40*, 261–279. [CrossRef]
32. Eastaugh, N.; Walsh, V.; Chaplin, T.; Siddall, R. Egyptian blue. In *The Pigment Compendium: Optical Microscopy of Historical Pigments*; Elsevier Butterworth Heinemann: Oxford, UK, 2004; pp. 147–148.
33. Kaczmarczyk, A.; Lahanier, C. Ancient Egyptian Frits and Coloured Faience Bodies: Problems of Classification. In *Application of Science in Examination of Works of Art*; England, P.A., Van Zelst, L., Eds.; Museum of Fine Arts: Boston, MA, USA, 1985.
34. Ibrahima, M.M.; Hassib, A.A.; Omara, S. Deterioration Aspects of the Egyptian Faience Ushabti. Statuette of the King Aspelta kept in Atfih Magazine, Egypt. *Adv. Res. Conserv. Sci.* **2022**, *3*, 1–14. [CrossRef]
35. Matin, M. Egyptian Faience glazing by the cementation method part 1: An investigation of the glazing powder composition and glazing mechanism. *J. Archaeol. Sci.* **2012**, *39*, 763–776. [CrossRef]
36. Abubakr, M.; Fouad, A.M. Color Alteration of Ancient Egyptian Blue Faience. *Int. J. Archit. Herit.* **2013**, *7*, 261–274. [CrossRef]
37. Helmi, F.; Abdel-Rehim, N. Study of Color Conversion By Time In Ancient Egyptian Faience Artifacts. *Sci. Cult.* **2016**, *2*, 17–23. [CrossRef]
38. Pradell, T.; Salvado, N.; Hatton, G.D.; Tite, M.S. Physical Processes Involved in Production of the Ancient Pigment, Egyptian Blue. *J. Am. Ceram. Soc.* **2006**, *89*, 1426–1431. [CrossRef]
39. Mao, Y. Lead-Alkaline Glazed Egyptian Faience: Preliminary Technical Investigation of Ptolemaic Period Faience Vessels in the Collection of the Walters Art Gallery. *J. Am. Inst. Conserv.* **2000**, *39*, 185–204. [CrossRef]
40. Nicholson, P.T. *Working in Memphis, The Production of Faience at Roman Period Kom Helul*; Egypt Exploration Society: London, UK, 2013.
41. Pradell, T.; Salvado, N.; Hatton, G.D.; Tite, M.S. Painting the Palace of Apries I: Ancient binding media and coatings of the reliefs from the Palace of Apries, Lower Egypt. *Herit. Sci.* **2018**, *6*, 1–20. [CrossRef]

42. Riccardelli, C. Egyptian Faience: Technology and Production. In *Heilbrunn Timeline of Art History*; The Metropolitan Museum of Art: New York, NY, USA, 2017. Available online: http://www.metmuseum.org/toah/hd/egfc/hd_egfc.htm (accessed on 1 April 2024).
43. Jaksch, H.; Seipel, W.; Weiner, K.L. Egyptian blue—Cuprorivaite a win-dow to ancient Egyptian technology. *Naturwissenschaften* **1983**, *70*, 525–535. [CrossRef]
44. Casolino, C.; Falcone, F.; Perna, M.G.; Metalla, E.; Rosatelli, G.; Stoppa, F.; Antonelli, S. Exploring Durrës between East and West: Discovery of a protostonepaste—Archaeological context and archaeometric analysis. *Heritage Sci.* **2024**, *12*, 84. [CrossRef]
45. Perna, M.G.; Falcone, F.; Casolino, C.; Metalla, E.; Rosatelli, G.; Antonelli, S.; Stoppa, F. Analysing the glaze of a medieval ceramic fragment from the Durres Amphitheater in Albania. *Herit. Sci.* **2024**, *12*, 82. [CrossRef]
46. Belousov, M.V.; Selivanov, E.N.; Gulyaeva, R.I.; Tyushnyakov, S.N.; Rakipov, D.F. Thermodynamics and kinetics of dolomite. *Izvestiya. Non-Ferr. Metall.* **2016**, *57*, 18–25. [CrossRef]
47. Tite, M.S.; Shortland, A.J.; Nicholson, P.T.; Jackson, C.M. The Use of Copper and Cobalt Colourants in Vitreous Materials in Ancient Egypt. In *La Couleur Dans La Peinture et L'Émaillage de L'Égypte Ancienne*; Colinart, S., Menu, M., Eds.; Edipuglia: Bari, Italy, 1998; pp. 112–113.
48. Colomban, P.; Kırmızı, B.; Simsek Franci, G. Cobalt and Associated Impurities in Blue (and Green) Glass, Glaze and Enamel: Relationships between Raw Materials, Processing, Composition, Phases and International Trade. *Minerals* **2021**, *11*, 633. [CrossRef]

Disclaimer/Publisher's Note: The statements, opinions and data contained in all publications are solely those of the individual author(s) and contributor(s) and not of MDPI and/or the editor(s). MDPI and/or the editor(s) disclaim responsibility for any injury to people or property resulting from any ideas, methods, instructions or products referred to in the content.